



Cite this: *Phys. Chem. Chem. Phys.*,  
2026, **28**, 3797

Received 28th October 2025,  
Accepted 12th January 2026

DOI: 10.1039/d5cp04142b

rsc.li/pccp

## Neat ionic liquids and deep eutectic solvents in photonics: *status quo* and future directions

Mila Miroshnichenko<sup>a</sup> and Pankaj Bharmoria<sup>ib</sup> \*<sup>ab</sup>

In the past decades, ionic liquids (ILs) and deep eutectic solvents (DESs) have gained recognition as green solvents, mainly because of their low vapor pressure, potential for recycling, and customized synthesis. The customization leverages task specificity for a particular application. While the photoactive ILs and DESs have been used as adjuvants in aqueous or organic solution for a variety of applications, this perspective article discusses the relatively underexplored applications of neat ILs or DESs in the field of photonics. Specifically, customization of their chemical structure is discussed to facilitate a particular linear and non-linear optical response, serving as a solvent-free photonic component, including future directions.

### Introduction

Ionic liquids (ILs), followed by deep eutectic solvents (DESs), have emerged as potential green solvents in the past two decades for multitude applications ranging from separation and purification,<sup>1,2</sup> protein-stability,<sup>3–5</sup> energy,<sup>6,7</sup> pharmaceuticals,<sup>8,9</sup> biotransformation,<sup>10,11</sup> detergency,<sup>12</sup> metal processing,<sup>13</sup> and electrochemistry.<sup>14,15</sup> This can be attributed to their properties including low vapour pressure, broad thermal ranges, recycling, biodegradability, specific solvation, and customized easy synthesis.<sup>16,17</sup> Neat ILs are salts comprising discrete organic cations associated with discrete organic or inorganic anions *via* weak electrostatic, H-bonding or London dispersion interactions below 100 °C.<sup>18</sup> Neat DESs consist of a eutectic mixture formed by Lewis or Brønsted acids and bases, which may encompass a diverse range of anion and/or cations. The liquidity of DESs at or near room temperature is supported by hydrogen bond interactions between the Lewis or Brønsted acid (donor), and Lewis base (acceptor).<sup>19</sup> While both ILs and DESs share similar physical properties, differences in their chemical properties contribute to their applications in diverse fields.<sup>20</sup> Photonics is one such field which requires specificity of the chemical nature of ILs or DESs. This is due to the fact that photonics involves the generation, detection, and manipulation of light; therefore, ions with a specific chemical structure can absorb, emit, and scatter the light. While both ILs and DESs offer advantage of the customization of the chemical structure, they have been underexplored in the field of photonics as neat-solvents. This

perspective article discusses the limited work reported in relation to the specific chemical structure of IL or DES components, as well as their implications in future linear and non-linear optical applications. For better understanding of the cross-disciplinary readership ILs and DESs and linear and non-linear optics are briefly described before the main discussion.

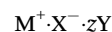
### Ionic liquids and deep eutectic solvents

An ionic liquid can be simply described using the following formula.



where  $M^+$  and  $X^-$  are discrete cations or anions associated mainly *via* weak electrostatic interactions due to steric hindrance caused by the organic cation or anion moiety.<sup>21</sup> For example, imidazolium cation based ILs;  $[C_4mim]^+Cl^-$  (m.p.  $\approx 70$  °C)<sup>22</sup> or  $[C_4mim]^+[C_8OSO_3]^-$  (m.p.  $\approx 37$  °C).<sup>23</sup> Here, replacement of  $Cl^-$  by a bulky  $[C_8OSO_3]^-$  creates steric hindrance to weaken the electrostatic interactions thereby decreasing the melting point (m.p.) see Fig. 1a. There are tens of discrete cations and anions which can be customized and combined in several combinations to obtain thousands of ILs, details of which can be availed from the cited ref. 24.

A deep eutectic solvent is a eutectic mixture with a lower melting temperature than that of its constituent components. It can be described using the following formula.<sup>25</sup>



where  $M^+$  is generally a nonsymmetric cation,  $X^-$  is a Lewis base and  $Y$  is a Lewis or Brønsted acid with a number  $z$ . For example, mixing  $[Cho]Cl$  (m.p.  $\approx 303$  °C) and  $NH_2CONH_2$  (m.p.  $\approx 134$  °C) in a 1:2 molar ratio leads to the formation of DES;  $[Cho]^+ \cdot Cl^- \cdot 2HNCONH_2$  has a lowered freezing temperature ( $T_f \approx 12$  °C) due to hydrogen bond interaction of urea with  $Cl^-$  (see Fig. 1b).<sup>26</sup> DESs can be of type I to IV

<sup>a</sup> The Institute of Materials Science of Barcelona, ICMA-B-CSIC, 08193 Bellaterra, Barcelona, Spain

<sup>b</sup> Department of Chemical Engineering, Universitat Politècnica de Catalunya, EEBE, Eduard Maristany 10-14, 08019 Barcelona, Spain.  
E-mail: pankaj.bharmoria@upc.edu



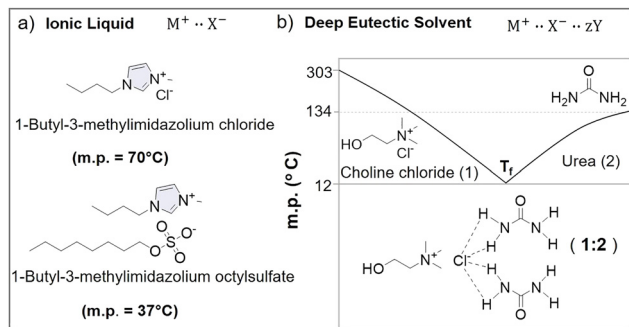


Fig. 1 Chemical equations and molecular structures of (a) ionic liquids and (b) deep eutectic solvents.

depending on their structure, the details of which can be obtained from the following cited ref. 27.

### Linear and non-linear optics

In linear optics, an incident light wave (generally weak) causes vibration of a molecule, followed by the emission of a light wave that has the same frequency as the incident light (Fig. 2a). Therefore, linear optics follows the superposition principle;  $A + B = X + Y$ ,<sup>28</sup> where  $A$  and  $B$  are input light waves hitting the molecule giving output light waves  $X$  and  $Y$  with the same frequency. Under the application of a weak electric field, the loosely bonded electrons in the materials undergo slight displacement from their equilibrium position to induce an electric dipole moment ( $\vec{P}(t)$ ). Since electrons near the nucleus are bound more strongly, their displacement potential is approximated as harmonic. Therefore, as per the harmonic approximation, the  $\vec{P}$  scales linearly with the electric field ( $\vec{E}$ ) amplitude of the incident light as per the following eqn (1).<sup>28,29</sup>

$$\vec{P}(t) = \epsilon_0 \chi \vec{E}(t) \quad (1)$$

where  $\vec{P}$  is the induced dipole moment per unit volume,  $\epsilon_0$  is the permittivity of the free space, and  $\chi$  is the polarization susceptibility. The common linear optical properties are reflection, refraction, scattering, and diffraction *etc.*

In non-linear optics, an intense light wave upon interaction with the molecule changes its optical properties such as frequency (Fig. 2b). Non-linear optics does not follow the superposition principle;  $A + B \neq X + Y$ , hence the optical properties like frequency, polarization and phase of the incident light undergoes change as the polarization density of the medium reacts non-linearly to the electric field of the light. Non-linearity is displayed by the molecules when the electric field strength of the light is high compared to the intra-atomic electric field *i.e.*  $E_a \approx 2 \times 10^7$  electrostatic unit.

Due to the strong electric field, the binding potential of electrons near the nucleus cannot be approximated as harmonic, resulting in large displacements from the equilibrium position. Therefore, the electron displacement does not scale linearly with the electric field as the non-linear electron motions become more significant. Hence, the induced polarization in non-linear optics is defined by eqn (2).<sup>30</sup>

$$\vec{P}_{NL} = \chi^{(1)} \vec{E} + \chi^{(2)} \vec{E}^2 + \chi^{(3)} \vec{E}^3 + \dots \quad (2)$$

where  $\chi^{(1)}$  is the linear polarization susceptibility of the materials and  $\chi^{(2)}$  and  $\chi^{(3)}$  are the non-linear polarization susceptibilities of the materials corresponding to the second and third order effects such as second and third harmonic generation, two or three photon absorption, triplet-triplet annihilation photon upconversion, and stimulated Raman scattering *etc.* Both NILs and DESs show different linear and non-linear optical responses compared to other solvents. This is due to their unique ionic nature, charge delocalization, customized heterogeneous polarity, and local microviscosity.

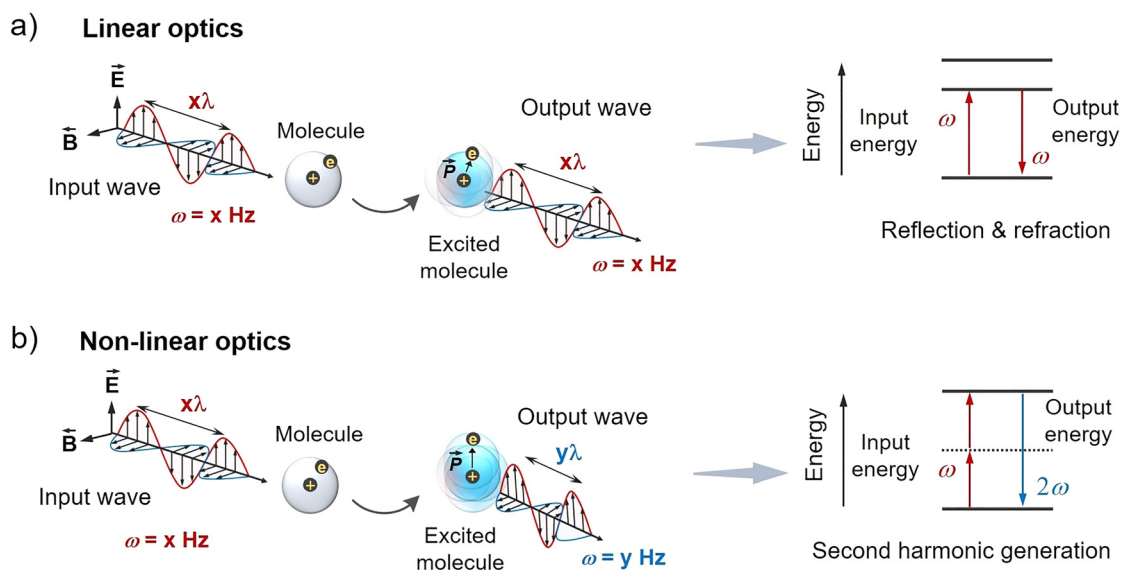


Fig. 2 Illustration of (a) linear and (b) non-linear optical responses of a molecule upon excitation with a linearly polarized light wave.  $\lambda$  = wavelength;  $\omega$  = frequency of the light wave.



## Heterogeneity, polarity and viscosity of ionic liquids and deep eutectic solvents

During the light–matter interaction in solution, the solvent polarity and viscosity play a crucial role in altering the photonic properties by influencing the electronic transitions and molecular dynamics.<sup>31</sup> The probability of electronic transition between different quantum states can be measured using the transition dipole moment integral eqn (3).<sup>32</sup>

$$\langle \mu \rangle_T = \int \psi_a^* \hat{\mu} \psi_b dr = \mu_T \quad (3)$$

where  $\langle \mu_T \rangle$  is the expectation value of the transition dipole moment vector ( $\hat{\mu}$ ) between the quantum states  $\psi_a^*$  and  $\psi_b$ , integrated over all coordinates,  $dr$ . If  $\mu_T \neq 0$ , transition is allowed (*e.g.* singlet to singlet transition), and when  $\mu_T = 0$ , transition is forbidden (*e.g.* singlet to triplet transition). The solvent polarity affects the transition dipole moment indirectly by altering the electronic distribution in the molecule in the ground and the excited state, which affects its interaction with light through induced polarization as per eqn (1)–(3) (Fig. 2). The nanoscale heterogeneity of ILs separates the ions into distinct polar and non-polar domains.<sup>33,34</sup> Polar domains are formed by charged headgroups of cations and anions, stabilized by electrostatic and hydrogen-bonding interactions, whereas non-polar domains are formed by aggregation of alkyl chains due to van der Waals interactions (Fig. 3).<sup>35</sup>

More importantly the length and structure of diversity in the polar/non-polar domain can be altered by changing the molecular structure of the cation or anion and their alkyl chain length.<sup>36,37</sup> For instance, the domain structure can vary from spatial heterogenous to liquid crystalline with an increase in the alkyl chain length.<sup>36</sup> The distinct structure, local environment, diffusion, reorientation and association dynamics of IL ions in different domains play a key role in governing the optical properties of them or of the molecules dissolved in them.<sup>38–41</sup> This is because the variations in polarity across

domains alters the stability of the ground and excited state of the molecule due to the different interaction energies of the solvent dipoles with the dipoles of excited chromophores leading to inhomogeneous spectral broadening and bathochromic or hypochromic spectral shifts.<sup>42</sup> Similar to NILs, DESs also exhibit differential polarity due to the heterogeneity in their structure which varies with the structure of their constituents.<sup>43–46</sup> The differential polarity can also affect the molecular solubility of chromophores to influence the absorption coefficients and emission lifetimes between different states.<sup>47</sup> The differential polarity of NILs and DESs can be investigated using Kamlet–Taft's solvent parameters ( $\alpha$ ,  $\beta$  and  $\pi^*$ ) using standard equations.<sup>48–50</sup> These parameters denote the hydrogen bond donor capacity ( $\alpha$ ), hydrogen bond acceptor capacity ( $\beta$ ), and polarizability ( $\pi^*$ ) of the liquid. Kamlet–Taft's parameters can be used to design ILs/DESs or their binary mixtures with specific polarity for a specific photonic application in the liquid-state. This is because the change in  $\alpha$ ,  $\beta$  and  $\pi^*$  affects both the solvation and diffusion of the dissolved chromophores, which affects both excited-state dynamics (monomer vs excimer emission) and energy transfer.<sup>51–53</sup> For example, aggregation induced emission enhancement (AIE), or quenching which are highly sensitive to solvent polarity.<sup>54–57</sup> In the case of AIE the molecular motions (rotation and vibrations) cease due to the packing of molecules in a certain geometry, which blocks the non-radiative decay ( $k_{nr}$ ) to boost the radiative decay ( $k_r$ ) to enhance the fluorescence quantum yield ( $\Phi_f$ ) according to the following eqn (4).

$$\Phi_f = \frac{k_r}{k_r + k_{nr}} \quad (4)$$

While AIE is specific to certain types of molecules, most of the chromophores show quenching of fluorescence due to aggregation induced by the change in concentration and solvent polarity. This is as per the Kasha rule which states that a small change in distance ( $R$ ) and angle ( $\theta$ ) between the transition dipole moment ( $\mu$ ) of neighbouring molecules in a medium of certain dielectric constant ( $\epsilon$ ) alters their inter-electronic coupling ( $J$ ) according to the following eqn (5).<sup>58</sup>

$$J = \frac{\mu^2(1 - 3 \cos^2 \theta)}{4\pi\epsilon R^2} \quad (5)$$

The close packing of dyes due to aggregation results in coupling to produce new electronic states like excimers with bathochromic or hypochromic shifts in the optical spectra with the quenching of fluorescence. Therefore, polarity and solvent chromophore interactions control chromophore aggregation due to solvophobic effects that can either lead to enhancement and quenching of fluorescence as per the type of the dissolved molecule.<sup>59</sup> That is why understanding of the Kamlet–Taft's parameters is important for designing the photoactivity of NILs or DESs. The issue of photoluminescence quenching can be addressed by the introduction of the fluorophore as a constituent of either NILs or DESs which can control the intermolecular interactions and solvophobicity by judicious choice of the counter ions. The suitable packing or co-assembly of molecules

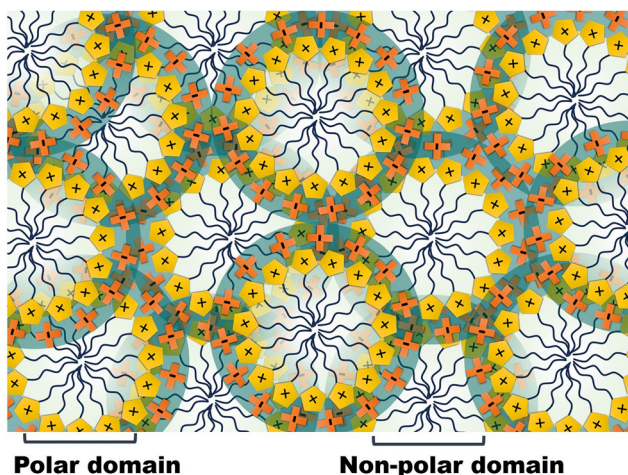


Fig. 3 Illustration of the segregated polar and non-polar domain in neat ILs. The domain length varies with an increase in the size of cation or anion headgroups and their alkyl chain length.



in such systems can maintain a specific angular distance to avoid excimer formation.<sup>60</sup>

Viscosity is another key property which influences the photonic properties of molecules by controlling the polarization, diffusion of chromophores and oxygen. The viscosity ( $\eta$ ) is related to the diffusion coefficient of a molecule ( $D$ ) in the solution *via* Stokes–Einstein eqn (6).<sup>61</sup>

$$D = \frac{k_B T}{6\pi\eta R} \quad (6)$$

where  $k_B T$  is the Boltzmann constant at a specific temperature ( $T$ ), and  $R$  is the radius of the a generally considered spherical particle in the solution. The higher viscosity tends to inhibit the non-radiative decay by restricting the collisions between the molecules and with ground state oxygen (triplet) thereby increasing the emission lifetimes and photo-stability.<sup>62</sup> The heterogenous structure of ILs or DESs changes with the change in alkyl chain, which alters the local bulk and shear moduli of the non-polar domains eventually altering the exciton diffusion.<sup>63,64</sup> Therefore, viscosity effects in both ILs and DESs can be highly domain specific as the dissolved molecule mostly experiences the local environment.<sup>65,66</sup> The understanding of the microviscosity is specifically important for the applications of ILs or DESs in photon upconversion processes involving triplet-states.<sup>67,68</sup> This is because the chromophore triplets can be quenched by the diffusing molecular oxygen which exists in the triplet-ground state. The higher local microviscosity can reduce diffusion of triplet-oxygen to enhance upconversion performance.<sup>69,70</sup> Since the viscosity affects the molecular polarization *via* dielectric relaxation time and bimolecular reaction rates *via* molecular collisions, it affects most of the diffusion dependent and solute–solvent interactions based optical processes.<sup>71–75</sup> Hence, understanding of the viscosity of NILs and DESs is important for their photonics applications. Details related to alteration in viscosity of both ILs and DESs due to the change in chemical structure can be obtained from the following ref. 76 and 77.

### Neat ionic liquids as photonic components

The customized nature of ILs leverage the possibility of engineering the chemical structures of both cation and anions for responding to the light waves of a specific energy due to electric field polarization.<sup>78</sup> However, the question, of what happens to NILs upon exposure to electromagnetic radiation of a specific wavelength is a key aspect of their photonic application,<sup>79</sup> considering the change in structural heterogeneity,<sup>80</sup> formation of possible transient photoexcited species,<sup>81,82</sup> and changes in the properties of the input wave.<sup>83</sup> The most common IL cation imidazolium  $[C_n\text{mim}]^+$  paired with an optically less active anion to leverage an inherent optical property in the broad UV-blue region.<sup>84</sup> The neat  $[C_n\text{mim}]^+$  paired with the  $\text{BF}_4^-$  anion shows absorption maxima at  $\sim 160$  and  $210$  nm with the tail extending into the 400 nm range.<sup>84</sup> However, their emission spectra display excitation wavelength dependent red shifts of the photoluminescence, known as the “red edge effect (REE) (Fig. 4a).”<sup>85,86</sup>

### Red Edge Effect

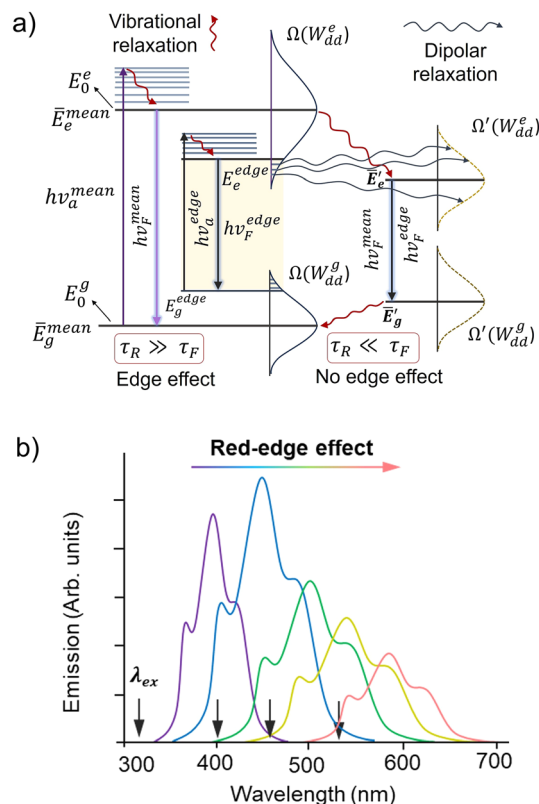


**Fig. 4** (a) Illustration of the modified Jablonski diagram showing electronic transitions, vibrational and dipolar relaxation during the red edge effect due to photoselection of certain chromophores experiencing different electric fields due to the interactions of dipoles of excited chromophores with the solvent dipole when excited at the edge of the absorption spectrum. (b) Illustration of the change in emission spectrum during the red-edge effect with a change in the excitation energy. (a) Was adapted from ref. 87 with permission from [Elsevier B.V.] [Demchenko, *Biophys. Chem.*, 1982, **15**, 101–10987], copyright 1982.

In REE the emission spectra undergo a red-shift when excitation is performed at longer wavelengths (Fig. 4a and b). The REE is generally observed in condensed inhomogeneous medium with high polarity and restricted motion, like at low temperature or at high viscosity where dielectric relaxation slows down with a shift to low frequency and longer relaxation times ( $\tau_R$ ).<sup>85,86</sup> In a typical case chromophores whose dipole moment and dipole orientation changes in the excited state ( $\mu_e$ ) with respect to the ground state ( $\mu_g$ ) show REE due to the interactions of medium dipole ( $\mu_m$ ) with the chromophore's dipoles (dipolar interactions). As a result, the chromophore experiences a different electric field with an added energy contribution from dipole–dipole interactions as per the following relationships.<sup>87</sup>

$$E = E_0 + \Omega(W_{dd}) \quad (7)$$

where  $E_0$  is the energy of unperturbed levels and  $\Omega(W_{dd})$  denotes distribution of the perturbations due to dipolar interactions with the medium. The  $W_{dd}$  is related to the mean dipole



moments of chromophores and medium as per the following relationships.<sup>87</sup>

$$W_{\text{dd}}^e \propto \bar{\mu}_e \cdot \langle \bar{\mu}_m \rangle \quad (8)$$

$$W_{\text{dd}}^g \propto \bar{\mu}_g \cdot \langle \bar{\mu}_m \rangle \quad (9)$$

For the edge excitation to occur, the  $W_{\text{dd}}^e$  should be maximum and  $W_{\text{dd}}^g$  should be minimum so that the dipolar interactions of the chromophores are minimum in the ground state and maximum in the excited state. It results in the photo selection of some chromophores with ground-state energy above  $E_a^{\text{edge}}$  and excited state energy below  $E_e^{\text{edge}}$  compared to the mean  $S_0$ - $S_1$  excitations. In this kind of case the  $\tau_R \gg \tau_F$  (Fig. 4a).

Fluorescent imidazolium based NILs due to the segregation of polar/non-polar ensembles create ground-state heterogeneity, with a local energetically distinct species having low 0-0 transition energy, moreover enhanced viscosity with the increase in chain length slow down the dielectric relaxation of other components around photo selected imidazolium causing the red-edge effect (Fig. 4b).<sup>88,89</sup> Moreover, these shifts become more prominent with an increase in the alkyl chain of the cation in neat IL ( $[\text{C}_2\text{mim}][\text{BF}_4] \sim 280 \text{ nm}$ ;  $[\text{C}_8\text{mim}][\text{BF}_4] \sim 390 \text{ nm}$ ).<sup>90</sup> While the red-edge spectroscopy is exploited to study the dynamics of proteins in an aqueous solution of various additives by excitation at the red-edge of the tryptophan absorbance,<sup>91</sup> considering the widespread use of neat imidazolium or pyridinium ILs in biocatalysis,<sup>92</sup> the red-edge effect of ILs<sup>93</sup> could be exploited as a probe to understand the structure-function relationship of enzymes upon cross-excitation at the red-edge of both tryptophan and neat ILs.

Besides inherent fluorescence, imidazolium cations have been chemically engineered with chiral emitters to display circularly polarized luminescence (CPL)<sup>94,95</sup> for application as a CPL emitter (Fig. 4c) in electrochemical cells. The CPL is a phenomenon where the chiral chromophore with luminescence dissymmetry ( $g_{\text{lum}}$ ) shows differential emission intensity of the right ( $I_R$ ) or left ( $I_L$ ) components of the circularly polarized light as per the following relationship (Fig. 5).<sup>96</sup>

$$g_{\text{lum}} = 2(I_L - I_R)/I_L + I_R \quad (10)$$

Besides being a CPL component, the NIL comprising tetrabutyl ammonium cation and chiral anions like prolinatate, valinate, and aspartate were used to induce CPL in the achiral europium triflate salt *via* coordination of anions with the europium (Fig. 5c).<sup>97</sup> Interestingly, the CPL spectra could be tuned according to the coordination of anions to  $\text{Eu}^{3+}$  highlighting the importance of customization.<sup>97</sup>

Other than cations, anion customization has also been exploited to achieve suitably photoactive NILs. For instance, pairing of allyl-imidazolium cations of varying chain lengths with fluorescent  $[\text{MnCl}_x\text{Br}_y]^{z-}$  anions resulted in phase change NILs with distinct thermochromic properties, which were exploited as sensors for temperature, relative humidity and alcohols by impregnating on the paper.<sup>98</sup> Kovalenko and co-workers paired photo-emissive lead halide anions with phosphonium cation as scintillators for application in fast neutron

## Circularly Polarized Luminescence

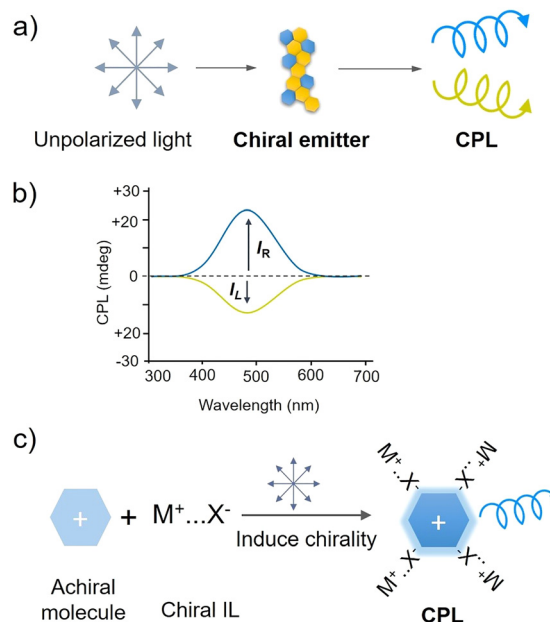


Fig. 5 Illustration of the circularly polarized luminescence. (a) Conversion of unpolarized light to the circularly polarized luminescent light by the chiral emitter, and (b) CPL spectra showing differential emission of the left and right circularly polarized light. (c) Induced CPL emission of an achiral compound upon mixing with a chiral ionic liquid.

imaging with recoil proton detection, with high resolution and low  $\gamma$ -ray sensitivity (Fig. 6).<sup>99</sup>

Neutron scintillation is an optical process where neutrons interact with the material to produce tiny flashes of light, detected further by the photomultiplier tube. These NILs exhibit specific properties such as proton rich cations, narrow excitation, low scattering, high photoluminescence quantum yield and large Stokes shift (1.7 eV) to avoid reabsorption desired for higher spatial resolution.<sup>99</sup> The H-rich cations of IL generate recoil protons upon bombardment with fast neutrons, forming electron-hole pairs upon interaction with anions, which show high PL emission *via* charge recombination (Fig. 6a).

Hisamoto and coworkers demonstrated Förster resonance energy transfer (FRET) in NIL, containing phosphonium cations, paired with sulfonated pyrene anions as the donor (D), and lipophilic fluorescein anions as the acceptor (A).<sup>100</sup>

FRET is a non-radiative energy transfer process that occurs *via* dipole-dipole interactions between the donor and acceptor molecules separated by  $<100 \text{ \AA}$ . As a result, the emission of the acceptor is increased at the expense of the donor's emission due to FRET (Fig. 7). The energy transfer efficiency ( $E$ ) in FRET can be estimated using the following relationship.<sup>28</sup>

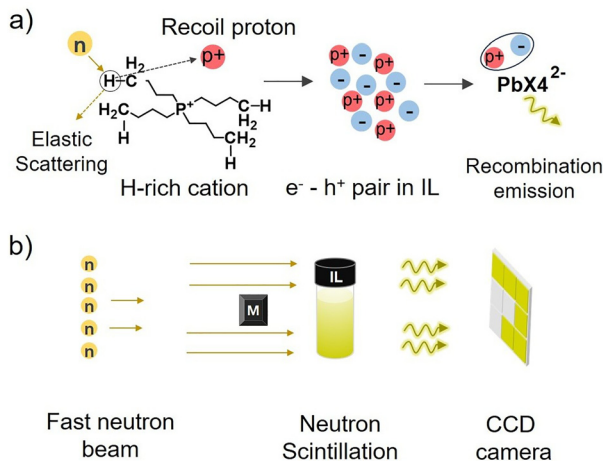
$$E = R_0^6/R_0^6 + r^6 \quad (11)$$

where  $r$  is the distance between the donor and acceptor and  $R_0$  is the Förster distance which signifies 50% energy transfer efficiency.

The FRET in the NIL mixture was utilized to form a solvent doped-PVC membrane with improved ion extraction-based



## Neutron Scintillation Imaging using NIL



sensing.<sup>100</sup> The liquid nature of the IL played a key role here for supporting the molecular diffusion of anionic chromophores (donor and acceptor), in the trapped FRET liquid for efficient energy transfer.

Kimizuka and co-workers demonstrated Dexter energy transfer (DET) in NIL comprising tetra-alkyl phosphonium cations and photoactive anions such as sulfonated anthracene and 4-(2-phenyloxazol-5-yl) benzene for green to blue, and blue to UV photon upconversion *via* triplet–triplet annihilation photon upconversion (TTA-UC)<sup>101–103</sup> (Fig. 8).

TTA-UC is a non-linear optical process that occurs in the annihilator's ensembles doped with a triplet photosensitizer in the oxygen free conditions. The photosensitizer upon excitation at low energy undergoes intersystem to the triplet-state and while coming back to the ground-state sensitize the annihilator triplets *via* triplet–triplet energy transfer. The sensitized annihilator triplets then undergo annihilation *via* spin-exchange coupling, resulting in the formation of an emissive singlet-state of the annihilator which show upconversion emission (Fig. 8a). The probability of singlet formation ( $f$ ) can be estimated using the following relationship.<sup>101</sup>

$$f = 2 \times \Phi_{UC} / \Phi_{isc} \cdot \Phi_{TET} \cdot \Phi_{TTA} \cdot \Phi_F \quad (12)$$

where  $\Phi_{UC}$ ,  $\Phi_{isc}$ ,  $\Phi_{TET}$ ,  $\Phi_{TTA}$ , and  $\Phi_F$  are the quantum yields of upconversion, intersystem crossing of the photosensitizer, triplet energy transfer from the photosensitizer to the annihilator, triplet–triplet annihilation and fluorescence quantum yield of the annihilator.

The high viscosity of NILs plays a key role in TTA-UC as it decreases the oxygen diffusion which protects chromophore triplets oriented between non-polar domains of the IL, from

## Förster Resonance Energy Transfer

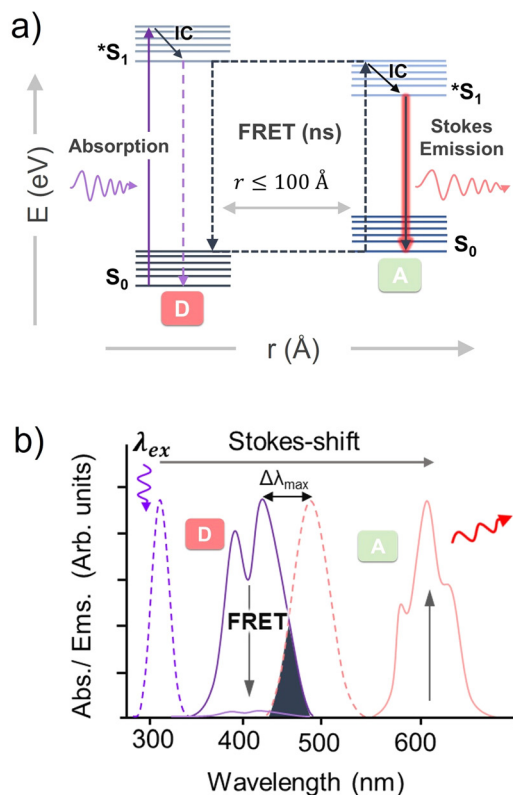


Fig. 7 (a) Illustration of the Förster resonance energy transfer through a modified Jablonski diagram. The excited donor while coming back to the ground state transfers energy to the acceptor if found within 100 Å radius, resulting in the amplification of an acceptor's emission at a longer wavelength. (b) Illustration of the change in the absorption and emission spectra of the donor and acceptor during FRET. IC = internal conversion or vibrational relaxation.

quenching by the ground state triplet oxygen in aerated conditions (Fig. 8c).<sup>101–103</sup> Moreover, the confinement of annihilators in contiguous ionic arrays allow effective triplet-energy transfer for an efficient energy upconversion.<sup>104</sup>

The customized nature of ILs has been exploited to generate laser pulses either in the bulk or confined liquid domain.<sup>105–108</sup> In an interesting report Kupfer and coworkers utilized the vibrational energy in the chemical bonds of NIL, ethyl-3-methylimidazolium dicyanamide ([C<sub>2</sub>mim][dca]) to generate nanosecond mid infra-red orange radiation (603 nm) by down-conversion of 532-nm laser pulses *via* molecular stimulated Raman scattering (SRS) (Fig. 9).<sup>105</sup>

SRS is a non-linear optical phenomenon that involves the inelastic scattering of photons from a coherently excited state of the Raman active material.

Consequently, the pump wavelength is transformed into Stokes and anti-Stokes wavelengths, which are shifted by the dominant bond vibrational frequency. The Raman frequency shift in SRS can be estimated using the following relationship.<sup>105</sup>

$$\omega_R = \omega_L \pm N_R \omega_v \quad (13)$$



## Dexter Energy Transfer in TTA-UC

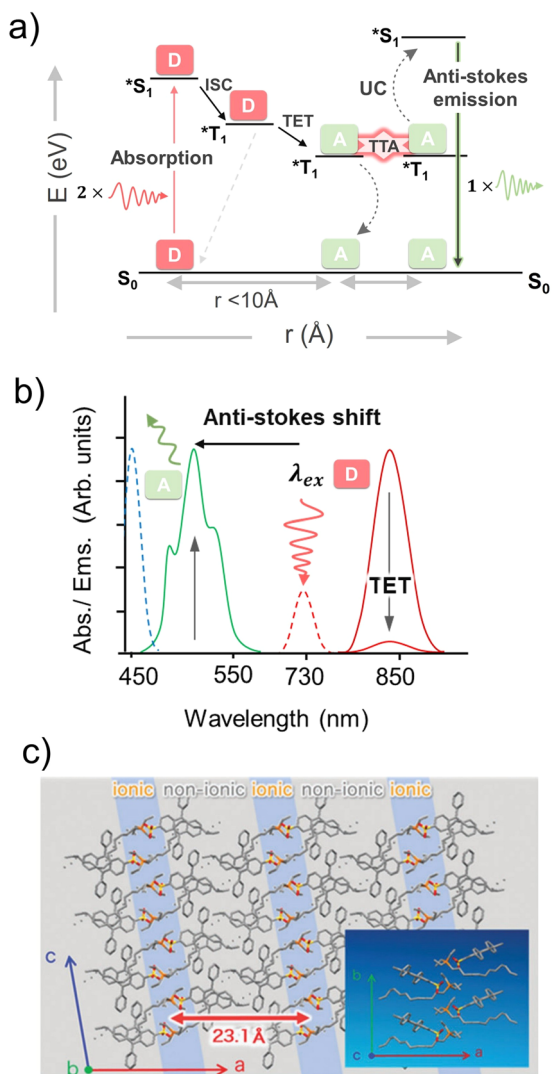


Fig. 8 (a) Illustration of the sequential energy transfer in TTA-UC. The sensitizer/donor upon absorption of low energy photons goes to the triplet-state *via* intersystem crossing (ISC), followed by the *r* triplet energy transfer to the annihilator (TET), which undergoes triplet-triplet annihilation (TTA), leading to the formation of an excited singlet-state of the annihilator, which show the anti-Stokes delayed emission. (b) Illustration of the change in emission spectra of photosensitizer and annihilator during TTA-UC. (c) Crystal structure of ionic crystals of  $[C_{14}(C_2)_3P]^+[DPASO_3]^-$  viewed along the *b*-axis, showing a lamellar structure consisting of ionic and non-ionic layers. Inset: The structure viewed along the *c*-axis to see a long tail alkyl chain sandwiched between two anthracene rings. (c) Has been reproduced from ref. 102 with permission from [The Royal Society of Chemistry, London] [Kimizuka *et al.*, *Phys. Chem. Chem. Phys.*, 2018, **20**, 3233–3240], copyright 2018.

where  $\omega_R$ ,  $\omega_L$ , and  $\omega_V$  are frequencies of the Raman shift, pump, and bond vibration, and  $N_R$  is the shift order in the case of the cascade process.

In the ethyl-3-methylimidazolium dicyanamide, the down converted emission corresponds to a Raman shift of  $2200\text{ cm}^{-1}$  due to dominant bond vibration of the dicyanamide anion at this frequency.<sup>105</sup>

## SRS in NIL to generate nanosecond laser pulse

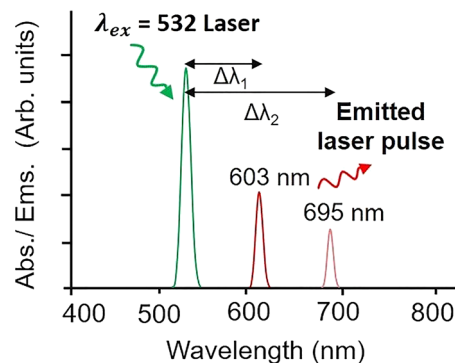


Fig. 9 Illustration of the spectral changes during photon downconversion of the 532 nm laser pulse due to stimulated Raman scattering in an IL;  $[C_2\text{mim}][\text{dca}]$  with Raman active dicyanamide anion. Adapted from ref. 105 with permission from [American Physical Society] [Palmer *et al.*, *Phys. Rev. Appl.*, 2023, **19**, 014052], copyright 2023.

Besides ethyl-3-methylimidazolium dicyanamide, molecular SRS was also observed with other NILs, comprising bis(trifluoromethylsulfonyl)amide anion paired with 1-butyl-1-methylpyrrolidinium and butylpyridinium cation for downconverting the 532 nm laser pulse to 578 nm, 599 and 632 nm *via* SRS.<sup>105</sup> Further customization of the NIL structure with a suitable Raman active cation or anion can also lead to SRS based energy upconversion to produce high frequency pulses with lifetimes varying between nano to femtoseconds.<sup>105</sup>

Sun and coworkers used the NIL, 1-butyl-3-methyl imidazolium hexafluorophosphate, as a gain medium to develop a microfluidic ionic liquid dye laser using BODIPY as the dye operating *via* whispering gallery modes (WGMs) based lasing emission.<sup>106</sup> WGM is an optical phenomenon generally observed in micro-sized circular resonators due to the circulation of light *via* total internal reflection along the curved boundary, resulting in the formation of resonance patterns.<sup>107,108</sup> The microdroplets of 1-butyl-3-methyl imidazolium hexafluorophosphate doped with BODIPY when pumped with 485 nm pulsed laser above the lasing threshold of  $40.1\text{ }\mu\text{J mm}^{-2}$  showed WGM-based lasing emission at 527 nm different from the normal fluorescence emission of BODIPY.<sup>106</sup> The refractive index and viscosity of the used IL played a key role to form droplets with optically smooth surfaces to avoid losses due to scattering during lasing.

NIL, Deng and coworkers reported electro-optical modulation by hydrophobic NILs, in the NIR region ( $\lambda = 1330$  or  $1530\text{ nm}$ ) under the application of a strong electric field ( $E = \pm 4\text{ V}$ ) due to N-H or C-H vibration and their overtone and combination transitions leading to radiationless deactivation or absorption in a microfluidic device.<sup>109</sup> The electro-optical modulation amplitude increased due to the change in carrier concentration near the electrodes with an increase in the electrical conductivity of ILs.

Borra and coworkers exploited the higher reflectance in the infra-red region, low vapour pressure under vacuum, and low



freezing temperature  $\sim 175$  K of silver coated NIL, 1-ethyl-3-methyl imidazolium ethylsulfate, to be used as a liquid mirror in an infra-red lunar telescope.<sup>110</sup> The reflectance ( $R$ ) is an optical property of the material indicating the fraction of light reflected in comparison to the transmitted light. The  $R$  depends on the angle of incidence ( $\theta$ ) and polarization of light ( $P$ ), and refractive index ( $n$ ) of the medium. The  $R$  of a liquid at  $\theta = 0^\circ$  can be calculated using the Fresnel equation.<sup>111</sup>

$$R = (n_1 - n_2 / n_1 + n_2)^2 \quad (14)$$

where  $n_1$  and  $n_2$  are the refractive index of air and liquid under study. The value of  $R$  varies between 0 and 1. However, the equation can change according to the change in the polarization and angle of incidence of the light.

Besides reflectance, the liquidity and surface tension<sup>112</sup> of NILs leverage the advantage of the shape change to create mirrors with high parabolic surfaces in microgravity. While it was considered a great breakthrough at that time, no further developments related to this were reported in the open literature until a recent internship report by Szobody *et al.*<sup>113</sup> The team conducted the work at NASA Goddard Space Flight Center to develop self-healing silver nanoparticle coated NIL mirrors for the next generation of liquid space telescopes.<sup>113</sup> This is an exciting, but highly underexplored area in NIL research with direct application in space exploration telescopes.<sup>114,115</sup> A representative image showing the reflection of NIR light by the IL coated silver nanoparticles is shown as Fig. 10.

Due to their nano-heterogeneous structure and polarizability NILs can diffract the light of a specific wavelength corresponding to the dimension of nano-heterogeneity.<sup>116</sup> This property makes the NILs a useful additive to increase the diffraction efficiency, resolution, and sensitivity of photopolymerizable hologram materials (Fig. 11).<sup>117,118</sup> Moreover customization of their viscosity makes them suitable diffusing solvents during photopolymerization.<sup>117,118</sup>

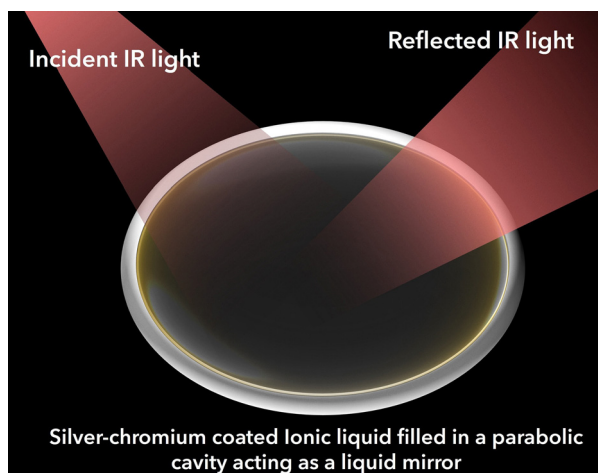


Fig. 10 Illustration of the infra-red reflectivity of silver and chromium coated ionic liquid filled in a parabolic cavity. The reflectivity increases in the infra-red region in the presence of ionic liquids compared to PEG, which can be used as a liquid mirror in the telescope.

## NIL as efficient diffractor for Holograms

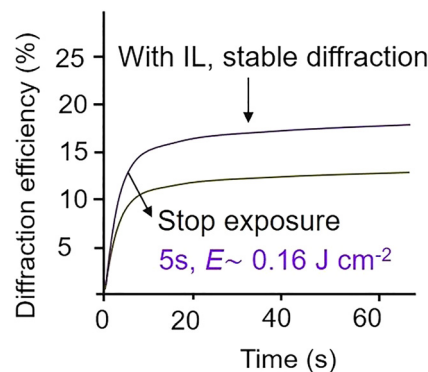


Fig. 11 Figure showing the improved diffraction efficiency of the photopolymerizable material with the addition of ionic liquids. Has been adapted from ref. 117 with permission from [AIP Publishing] [Veith *et al. Appl. Phys. Lett.*, 2008, **93**, 141101], copyright 2008.

## Neat deep eutectic solvents as photonic components

Similar to ILs, the customized nature of DESs can be exploited to develop photo-responsive DESs by substitution of one of the components with a photoactive molecule. Neat DESs (NDESS) are considered next generation green solvents as replacements for ILs due to similarities in their physical properties.<sup>20,27</sup> However, unlike NILs, NDESS have been less explored in photonics which gives an opportunity to develop this field. The refractive index (linear or non-linear) is among the most significant optical properties of DESs which leverage their potential applications as a medium for liquid-based optical communications.<sup>119-121</sup> The non-linear refractive index ( $n_2$ ) varies with the light intensity ( $I$ ) as per the following eqn (15).<sup>121</sup>

$$n - n_0 = \Delta n = n_2 I \quad (15)$$

Furthermore, it is related to the third order non-linear susceptibility ( $\chi^{(3)}$ ) as per eqn (16).<sup>121</sup>

$$n_2 = \frac{3\chi^{(3)}}{4\epsilon_0 c n^2} \quad (16)$$

where  $\epsilon_0$  is the relative permittivity of free space and  $c$  is the velocity of light. Experimentally it can be measured using the Z-scan technique.<sup>122</sup> Some DESs such as [Cho]Cl:lactic acid, show a negative third order non-linear refractive index which can support bright optical solitons over long distances to improve the performance of long-distance optical communication.<sup>121</sup> This is due to the structural heterogeneity of DESs that creates localized structural domains smaller than the wavelength of excitation light. The negative non-linear refractive index arises due to the thermal lensing effect<sup>123</sup> caused by heating of the excitation spot by a high energy laser pulse than the edges, thus creating a refractive index gradient due the temperature gradient caused by the localized heating. Interestingly, the customized nature leverages tuning of the magnitude of the negative non-linear refractive index of DESs by changing the ratio and structure of HBD and HBA. Considering the available HBA or HBD, and their customized nature, thousands of DESs,



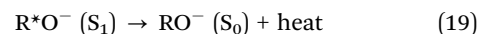
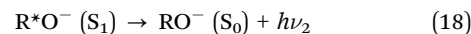
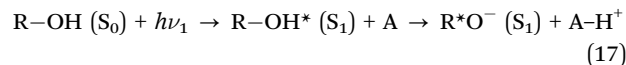
supporting bright optical soliton can be synthesized for enhanced optical communication.

Gupta and coworkers developed a fluorescent NDESS (heptyltriphenylphosphine ( $M^+$ ), bromide ( $X^-$ ), and decanoic acid ( $zY$ )) which were used as sensors to detect  $D_2O$  *via* an increase in fluorescence intensity.<sup>124</sup> Hopkins and coworkers exploited the customized nature of DESs to synthesize chiral DESs comprising alkylammonium chloride salts as HBA and a chiral HBD (amino acids, organic acids and monosaccharide) to leverage the CPL property to a racemic mixture of luminescent dissymmetric lanthanide complexes.<sup>125,126</sup> Further changing the HBA with alkylphosphonium chloride enhanced the enthalpy and entropy of chiral discrimination by 50%, demonstrating the advantage of the customized nature of DESs.<sup>127</sup>

Murakami and co-workers exploited the thermal stability of DESs as solvents to host organic chromophores (PtOEP, PdOEP and DPA) to achieve high efficiency upconversion of green photons to blue photons.<sup>128</sup> Unlike the IL-based TTA-UC system where chromophores were part of the IL structure,<sup>101–104</sup> DESs have been used just as native solvents. However, advancements can be made in this direction by introducing the HBD property to the TTA-UC chromophores to develop solvent free TTA-UC DESs.

The dynamic heterogeneity, hydrogen bond acidity or basicity of NDESSs has also been exploited to study excited state

proton-transfer (ESPT) operating at the nanosecond timescale using either pyranine or naphthol's as proton-transfer probes.<sup>129,130</sup> ESPT is a photochemical process where a proton rapidly shifts within a molecule after absorbing light, creating a new, tautomeric form with different fluorescence or vibrational spectra.<sup>131</sup> ESPT can be understood using the following equations.<sup>131</sup>



where  $R-OH$  and  $A$  represent the proton donor and acceptor. The deprotonated molecule in the excited singlet state ( $S_1$ ) can relax to the ground state *via* radiative ( $h\nu_2$ ) or vibrational relaxation *via* non-radiative (heat) emission. Since ESPT involves proton transfer, the DESs comprising of HBD and HBA can directly participate in the process.<sup>129</sup> Guchhait and coworkers also exploited the dynamic heterogeneity of DESs and reported ESPT at the nanosecond timescale (2.6 to 7.5 ns) using pyranine as the proton donor in the DESs,  $[(C_2)_4N]^+[Br]^-:(CH_2OH)_2$ ,  $[(C_2)_4N]^+[Br]^-:Glycine$ ,  $[(C_2)_4N]^+[Cl]^-:(CH_2OH)_2$ ,  $[Cho]^+[Cl]^-:(CH_2OH)_2$  confined inside the supported liquid membrane due to long-range interfacial order effects. The long-range interfacial

**Table 1** Summary of neat ionic liquids and deep eutectic solvents and their specific properties exploited for photonics

Neat ionic liquid	Photonic property	Properties of NIL exploited
$[C_{2-8}mim]^+[BF_4]^-$ and $[C_4mim]^+[PF_6]^-$	Optical absorption and emission	Customization, and polarity <sup>84</sup>
$[C_nmim]^+[X]^-$ ( $n = 2, 4, 8$ ; $X = Cl, BF_4, PF_6$ )	Red edge effect	Heterogeneity, polarity and viscosity <sup>88–90,93</sup>
$[C_nmpy]^+[X]^-$ ( $n = 3, 4, 8$ ; $X = BF_4, N(CN)_2$ )		
$[C_{nr}mim]^+[R]^-$ ( $R =$ diphenylacrylonitrile; $n = 1, 7, 11$ )	Circularly polarized luminescence	Structural customization, chirality <sup>94,95,97</sup>
$[C_2TCBNim]^+[PF_6]^-$ , $[(C_4)_4N]^+[X]^-$ ( $X = Pro, Val, Asp$ )		
$[C_{14}(C_6)_3P]^+[PbX_4]^-$ , $[(C_4)_4P]^+[PbX_4]^-$	Neutron scintillation	Proton richness, viscosity, low scattering <sup>99</sup>
$[C_{14}(C_6)_3P]^+[X]^-$ ( $X = HP-SO_3, C_{12}-FL$ )	Förster resonance energy transfer	Structure customization, viscosity, polarity <sup>100</sup>
$[C_{14}(C_6)_3P]^+[DPASO_3]^-$ , $[C_{14}(C_2)_3P]^+[DPASO_3]^-$	Dexter energy transfer in TTA-based photon upconversion	Structure customization, heterogeneity, viscosity, thermal stability, polarity <sup>101–104</sup>
$[C_{14}(C_6)_3P]^+[PPOSO_3]^-$	Stimulated Raman scattering based photon up and down conversion	Structure customization, thermal stability <sup>105</sup>
$[C_2mim]^+[N(CN)_2]^-$ , $[X]^+[NTf_2]^-$ ( $X = C_4mPyr, C_4Pyr$ )	Gain medium in microfluidic dye laser operational <i>via</i> whispering gallery modes	Refractive index, and viscosity <sup>106</sup>
$[C_4mim]^+[PF_6]^-$	Electro-optical modulation	Conductivity, viscosity, electrochromic window <sup>109</sup>
$[C_nmim]^+[X]^-$ ( $n = 1$ or $4$ ; $X = NTf_2, BF_4, ClO_4, PF_6, N(CN)_2$ )	Reflectance	Liquidity, refractive index, surface tension, low vapour pressure, broad thermal range <sup>110,112</sup>
$[C_2mim]^+[C_2OSO_3]^-$		Heterogeneity, polarizability, viscosity <sup>117,118</sup>
$[C_4mim]^+[PF_6]^-$ and $[C_4mim]^+[BF_4]^-$	Diffraction	
Neat deep eutectic solvent	Photonic property	Properties of DES exploited
$[Cho]^+[Cl]^-$ : lactic acid	Negative non-linear refraction due to the thermal lensing effect	Negative refractive index, heterogeneity, liquidity <sup>121</sup>
Heptyltriphenylphosphine bromide: decanoic acid	Fluorescence	Structural customization, polarity <sup>124</sup>
$[C_4)_4N]^+Cl^-$ : $zY$ ( $zY = D-(+)-\alpha$ -glucose; $D-(+)-\beta$ -glucose; $L-(-)-\alpha$ -glucose; $D-(-)-\beta$ -fructose). $[C_4)_4N]^+Cl^-$ : $zY$ : $zY$ or $[Cho]Cl$ : $zY$ ( $zY = L$ -lactic acid, $L$ -leucic acid, $L$ -ascorbic acid, $R/S$ -acetoxypropionic acid, and methyl- $(S)$ -lactate). $[C_4)_4N]^+Cl^-$ or $[C_4)_4P]^+Cl^-$ : $zY$ ( $zY = L$ - or $D$ -glutamic acid, $L$ -proline, and $L$ -arginine).	Circularly polarized luminescence	Structural customization, chirality <sup>125–127</sup>
$[C_n)_4N]^+Cl^-$ : decanoic acid ( $n = 4$ or $8$ )	Dexter energy transfer in TTA-based photon upconversion	Liquidity, polarity, thermal stability <sup>128</sup>
$[M]^+[X]^-$ : $zY$ ( $M = [(C_2)_4N$ or $Cho$ ; $X = Cl$ or $Br$ ; $zY =$ ethylene glycol, or glycine or urea or tetraethylene glycol)	Excited-state proton transfer	Hydrogen bond acidity, liquidity, nano-heterogeneity and polarity <sup>130,131</sup>



order in the confined domain was confirmed from slow dynamics of solvent relaxation and the red-edge effect.<sup>130</sup>

## Conclusions

The customized nature of NILs by large, and NDESSs to some extent, has been exploited for chemical engineering of their structure for a specific linear or non-linear optical application. These processes include the red-edge effect, circularly polarized luminescence, neutron scintillation, photon conversion *via* FRET, DET, stimulated Raman scattering, electro-optical modulation, micro-fluidic dye lasers, reflector for liquid mirrors, directors in holograms, and refractors for liquid-based optical communication and medium for ESPT. However, these studies are limited to the proof-of-concept level, though with potential applications discussed in the respective sections. Other than the photonic part, properties like viscosity, polarity, and refractive index, broad thermal range, structural heterogeneity, conductivity, large electrochromic window and hydrogen bond acidity or basicity play a key role in their successful implementation in the reported photonic systems, as summarized in Table 1. Upon evaluation of the use of NDESSs in comparison to NILs within photonic systems, it becomes evident that NDESSs are still in the early stages of development, despite sharing numerous physicochemical characteristics with NILs. They are regarded as an advanced version of NILs primarily due to their environmental sustainability, which is attributed to their low toxicity, biodegradability, and low-cost synthesis.<sup>132</sup> While these attributes may provide NDESSs with certain advantages over NILs in certain applications, the requirements for many photonic applications necessitate photoactive materials that exhibit excellent photostability along with broad absorption and emission ranges. Consequently, one of the essential components must include either a polyaromatic hydrocarbon (which is typically considered toxic), metals,<sup>133</sup> semiconductor nanoparticles,<sup>134,135</sup> or perovskite compounds (may use toxic metals like Pb and Cd)<sup>136,137</sup> and carbon nanoparticles.<sup>138,139</sup> NIL also offers great structural versatility to design photoactive ionic liquids with a vast number of polyaromatic organic cations or anions because of its two-component nature. Whereas the structural complexity of DESs due to the multicomponent nature held together by hydrogen bonding limits its versatility beyond bio-derived components. Therefore, currently NILs are leading the photonic applications in the neat form compared to NDESSs. However, the sustainable nature of DESs is of high value compared to NILs when considered only as solvents to disperse photoactive compounds to study various optical processes,<sup>128,130,131</sup> followed by easy separation at the end-of-life. For consideration purely as a photonic component more NDESSs with polyaromatic dyes as one of the components need to be synthesized for a valid comparison with NILs in photonic applications.

## What is next for NILs and DESs in photonics?

Thermal stability is among the key properties of NILs and DESs to be exploited in photonics, as it can address the heating

effects during light-matter interactions.<sup>140–143</sup> Heating can negatively alter the optical properties, such as resonance frequencies, and signal integrity due to the thermal cross-talk and change in the refractive index to affect the device performance.<sup>144</sup> However, the higher heat capacities of NILs and DESs can serve as a heat sink in the case of thermo-optical effects. The studies on photonics in the liquid-state (chemical or metallic liquids) are slowly gaining momentum.<sup>145,146</sup> NILs and DESs can contribute immensely as an organic liquid to this, with the customizable nature of their thermophysical and chemical properties. For example, liquid water, due to its absorption in the tetra-hertz range, generates a broadband terahertz wave.<sup>145,146</sup> In case of liquid gallium, the high plasma frequency has been exploited to realize ultra-violet plasmonic structures.<sup>147</sup> In case of liquid metal nanostructures, the absence of domain boundaries and the smoothness of surfaces results in an extended carrier relaxation time, consequently leading to reduced losses for surface plasmons in addition to broad thermal ranges.<sup>148</sup> Along similar lines, NILs and DESs can be explored as liquid organic/inorganic semiconductors<sup>149,150</sup> by synthesizing the variants comprising polyaromatic hydrocarbons and liquid metal salts. While a few proof-of-concept studies, especially on NILs, have already been reported in this direction,<sup>103,104</sup> broadening the scope of detailed fundamental investigations related to applicable photonics can further attract the attention of the scientific community in this direction. For instance, the feasible advancement of liquid-junction solar cells<sup>151</sup> or liquid solar cells<sup>152</sup> as a sustainable clean energy alternative could significantly enhance the use of NIL or DES-based liquid organic semiconductors as *in situ* photon converters<sup>103,104,153,154</sup> or solar concentrators<sup>155,156</sup> to capture light either below or above the solar cell's band gap, thereby improving performance.<sup>155–158</sup> While both NILs and DESs have been used as electrolyte or redox mediators in dye sensitized solar cells (DSSCs)<sup>159–161</sup> due to their conductivity and non-volatility, using them as a dye, electrolyte and redox mediator in a single system would be an ideal advancement in this direction. For example, anthracene-based dyes have been used as dye and photon upconverters in DSSCs,<sup>157</sup> hence suitable NDESSs and NILs comprising redox active dyes if synthesized can serve both as sensitizer dyes, photon converters, and redox mediators in DSSCs. Both NILs and NDESSs possess suitable properties for applications in liquid luminescent solar concentrators.<sup>162</sup> For example, the high refractive index, heterogenous structure, differential polarity to solubilize luminophores and more importantly structural tunability to design liquids containing luminophores with high Stokes-shifts and thermal stability. Despite having suitable properties NILs<sup>163,164</sup> or DESs have been rarely investigated for LSCs. With the emergence of liquid based LSCs, both NILs and NDESSs could become promising future candidates for LSCs if suitable design principles considering the photostability of luminophores are envisioned. Owing to their thermochemical phase change characteristics, both NILs and DESs exhibit significant potential as materials for thermal energy storage.<sup>165–167</sup> Molecular solar thermal energy storage systems (MOST) are emerging as clean energy alternatives where solar energy is stored as heat in molecular photoswitches.<sup>168–170</sup> Besides fundamental



research, recent years have seen a lot of reports on the development of MOST devices,<sup>167,171</sup> in which photoswitches were dissolved in organic solvents (generally toxic), and were tested at different flow-rates, and residence-times to absorb maximum solar photons to be stored as heat by the photosomer.<sup>172</sup> A typical example of MOST is the norbornadiene (NBD) ↔ quadricyclane (QC) system, where NBD, after absorbing UV photons, gets converted to the QC form, which stores heat as high as 93 kJ mol<sup>-1</sup>.<sup>169</sup> Besides NBD, several other organic photoswitches like azobenzene, azopyrazole, dihydroazulene, and *ortho*-dianthrylbenzenes are emerging as suitable solar-thermal energy storage materials.<sup>169,173</sup> As a green alternative to organic solvents, mixtures of water and non-ionic surfactants have been explored at high NBD concentrations, generally needed to store higher energy.<sup>174</sup> However, water–surfactant mixtures are prone to phase separation above a certain concentration of the photoswitch or surfactant due to the solubility limitations. NILs or NDESs can overcome the solubility limitations as the photoswitches can be transformed directly into thermally stable NILs or DESs with required viscosities and vapor pressure through appropriate chemical engineering. This transformation can lead to improved heat storage capabilities, as it combines the heat storage resulting from the phase change in NILs or DESs with the heat absorbed from solar photons by the photoswitches.

## Author contributions

P. B. conceived the idea of this perspective article, wrote the first draft and revised the manuscript. M. M. assisted in editing the manuscript.

## Conflicts of interest

There are no conflicts to declare.

## Data availability

Supplementary information is available. See DOI: <https://doi.org/10.1039/d5cp04142b>. The Supplementary information Table S1, contains full names of the abbreviations used in this manuscript.

All figures presented in this manuscript were prepared by the authors themselves and any information related to their drawing is available from the corresponding author upon reasonable request by email. Appropriate references have been cited where needed in relation to the presented figures.

## Acknowledgements

P. B. acknowledges the Ramón y Cajal grant from the Spanish State Investigation Agency (grant no. J03416) and La-Caixa junior research leadership-post doctoral project PHOLCEB (ID: 100010434, fellowship code: LCF/BQ/P122/11910023) for financial support. M. M. and P. B. acknowledge the State Investigation Agency, through the Severo Ochoa Programme

for Centres of Excellence in R&D (CEX2023-001263-S) and project PID2021-123873NB-I00 for financial support.

## Notes and references

- 1 S. P. M. Ventura, F. A. Silva, M. V. Quental, D. Mondal, M. G. Freire and J. A. P. Coutinho, *Sep. Sci.*, 2016, **39**, 3505–3520.
- 2 P. Bharmoria, A. A. Tietze, D. Mondal, T. S. Kang, A. Kumar and M. G. Freire, *Chem. Rev.*, 2024, **124**, 3037–3084.
- 3 N. Yadav and P. Venkatesu, *Phys. Chem. Chem. Phys.*, 2022, **24**, 13474–13509.
- 4 A. Sanchez-Fernandez, J. H. Nicholson, S. M. M. Huaman, C. A. Romero, J.-F. Poon, S. Prevost and A. P. S. Brogan, *Commun. Chem.*, 2025, **8**, 173.
- 5 T. Zhou, C. Gui, L. Sun, Y. Hu, H. Lyu, Z. Wang, Z. Song and G. Yu, *Chem. Rev.*, 2023, **123**, 12170–12253.
- 6 S. Chattopadhyay, S. Kataria, S. Prusty, M. S. ubban, A. Kumar and S. Sutradhar, *ACS Symp. Ser.*, 2025, **1504**, 135–153.
- 7 R. M. Moshikur, M. R. Chowdhury, M. Moniruzzaman and M. Goto, *Green Chem.*, 2020, **22**, 8116–8139.
- 8 E. Chevé-Kools, Y. H. Choi, C. Roullier, G. Ruprich-Robert, R. Grougnet, F. Chapeland-Leclerc and F. Hollmann, *Green Chem.*, 2025, **27**, 8360–8385.
- 9 Q. Hou, X. Qi, M. Zhen, H. Qian, Y. Nie, C. Bai, S. Zhang, X. Baia and M. Ju, *Green Chem.*, 2021, **23**, 119–231.
- 10 Y. Gu and F. Jérôme, *Chem. Soc. Rev.*, 2013, **42**, 9550–9570.
- 11 P. Bharmoria, M. J. Mehta, I. Pancha and A. Kumar, *J. Phys. Chem. B*, 2014, **118**(33), 9890–9899.
- 12 E. L. Smith, A. P. Abbott and K. S. Ryder, *Chem. Rev.*, 2014, **114**, 11060–11082.
- 13 D. R. MacFarlane, M. Forsyth, P. C. Howlett, J. M. Pringle, J. Sun, G. Annat, W. Neil and E. I. Izgorodina, *Acc. Chem. Res.*, 2007, **40**, 1165–1173.
- 14 Z. Liu, F. Feng, W. Feng, G. Wang, B. Qi, M. Gong, F. Zhang and H. Pang, *Energy Environ. Sci.*, 2025, **18**, 3568–3613.
- 15 S. Zhang, N. Sun, X. He, X. Lu and X. Zhang, *J. Phys. Chem. Ref. Data*, 2006, **35**, 1475–1517.
- 16 D. Yu, Z. Xue and T. Mu, *Chem. Soc. Rev.*, 2021, **50**, 8596–8638.
- 17 K. Fumino, S. Reimanna and R. Ludwig, *Phys. Chem. Chem. Phys.*, 2014, **16**, 21903–21929.
- 18 L. J. B. M. Kollau, M. Vis, A. van den Bruinhorst, A. C. C. Esteves and R. Tuinier, *Chem. Commun.*, 2018, **54**, 13351–13354.
- 19 H. Zhang, J. M. Vicent-Luna, S. Tao, S. Calero, R. J. J. Riobóo, M. L. Ferrer, F. del Monte and M. C. Gutiérrez, *ACS Sustainable Chem. Eng.*, 2022, **10**, 1232–1245.
- 20 R. Hayes, G. G. Warr and R. Atkin, *Chem. Rev.*, 2015, **115**, 6357–6426.
- 21 D. Lengvinaitė, S. Kvedaravičiute, S. Bielskutė, V. Klimavičius, V. Balevičius, F. Mocci, A. Laaksonen and K. Aidas, *J. Phys. Chem. B*, 2021, **125**, 3255–13266.



- 22 María J. Dávila, S. Aparicio, R. Alcalde, B. García and J. M. Leal, *Green Chem.*, 2007, **9**, 221–232.
- 23 A. A. Bodour, N. Alomari, G. P. Duran, S. Rozas, G. I. Silva, S. Aparicio, A. G. Vega and M. Atilhan, *Energy Fuels*, 2025, **39**, 12791–12829.
- 24 Z. Lei, B. Chen, Y.-M. Koo and D. R. MacFarlane, *Chem. Rev.*, 2017, **117**, 6633–6635.
- 25 B. B. Hansen, S. Spittle, B. Chen, D. Poe, Y. Zhang, J. M. Klein, A. Horton, L. Adhikari, T. Zelovich, B. W. Doherty, B. Gurkan, E. J. Maginn, A. Ragauskas, M. Dadmun, T. A. Zawodzinski, G. A. Baker, M. E. Tuckerman, R. F. Savinell and J. R. Sangoro, *Chem. Rev.*, 2021, **121**, 1232–1285.
- 26 J. A. Sirviö, M. Visanko and H. Liimatainen, *Green Chem.*, 2015, **17**, 3401–3406.
- 27 V. Pandey, T. Pandey and R. S. Kaundal, Deep Eutectic Solvents ACS Symposium Series 2025, vol. 1504, ch. 3, pp. 77–95.
- 28 P. Bharmoria and S. P. M. Ventura, Optical Applications of Nanomaterials, in *Nanomaterials for healthcare, energy, and environment. Advanced structured materials*, ed. A. Bhat, I. Khan, M. Jawaid, F. Suliman, H. Al-Lawati and S. Al-Kindy, vol. 118, Springer, Singapore, 2019.
- 29 <https://www.chem.uci.edu/~potma/lecture3.pdf>.
- 30 G. Agrawal, *Nonlinear fiber optics*, Elsevier Inc., 5th edn, 2013, ch. 1, pp. 1–25.
- 31 S. L. Bondarev, V. N. Knyukshto and S. A. Tikhomirov, *J. Appl. Spectrosc.*, 2002, **69**, 230–237.
- 32 Transition moment in IUPAC Compendium of Chemical Terminology, International Union of Pure and Applied Chemistry, 5th edn, 2025.
- 33 R. Hayes, G. G. Warr and R. Atkin, *Chem. Rev.*, 2015, **115**, 6357–6426.
- 34 M. Sha, Y. Liu, H. Dong, F. Luo, F. Jiang, Z. Tang, G. Zhu and G. Wu, *Soft Matter*, 2016, **12**, 8942–8949.
- 35 Y.-L. Wang, B. Li, S. Sarman, F. Mocci, Z.-Y. Lu, J. Yuan, A. Laaksonen and M. D. Fayer, *Chem. Rev.*, 2020, **120**, 5798–5877.
- 36 Y. Ji, R. Shi, Y. Wang and G. Saielli, *J. Phys. Chem. B*, 2013, **117**, 1104–1109.
- 37 M. Torkzadeh and M. Moosavi, *J. Phys. Chem. B*, 2020, **124**, 11446–11462.
- 38 Z. Hu and C. J. Margulis, *Proc. Natl. Acad. Sci. U. S. A.*, 2006, **103**, 831–836.
- 39 V. H. Paschoal, L. F. O. Faria and M. C. C. Ribeiro, *Chem. Rev.*, 2017, **117**, 7053–7112.
- 40 T. Frömbgen, K. Drysch, T. Tassaing, T. Buffeteau, O. Hollóczki and B. Kirchner, *Angew. Chem., Int. Ed.*, 2025, **64**, e202502885.
- 41 P. Oulevey, S. Lubner, B. Varnholt and T. Bürgi, *Angew. Chem., Int. Ed.*, 2016, **55**, 11787–11790.
- 42 A. Marini, A. M. Losa, A. Biancardi and B. Mennucci, *J. Phys. Chem. B*, 2010, **114**, 17128–17135.
- 43 S. Spittle, D. Poe, B. Doherty, C. Kolodziej, L. Heroux, M. A. Haque, H. Squire, T. Cosby, Y. Zhang, C. Fraenza, S. Bhattacharyya, M. Tyagi, J. Peng, R. A. Elgammal, T. Zawodzinski, M. Tuckerman, S. Greenbaum, B. Gurkan, C. Burda, M. Dadmun and E. J. M. Joshua Sangoro, *Nat. Commun.*, 2022, **13**, 219.
- 44 M. N. Kamar, A. Mozhdzhehi, B. Dupont, R. Lefort, A. Moréac, J. Ollivier, M. Appel and D. Morineau, *J. Chem. Phys.*, 2025, **163**, 134506.
- 45 A. Malik and H. K. Kashyap, *Phys. Chem. Chem. Phys.*, 2023, **5**, 19693–19705.
- 46 T. Rinesh, H. Srinivasan, V. K. Sharma, V. García Sakai and S. Mitra, *J. Chem. Phys.*, 2025, **162**, 244503.
- 47 R. K. Venkatraman and A. J. Orr-Ewing, *Acc. Chem. Res.*, 2021, **54**, 4383–4394.
- 48 X. Wang, S. Zhang, J. Yao and H. Li, *Ind. Eng. Chem. Res.*, 2019, **58**, 7352–7361.
- 49 M. A. Ab Rani, A. Brant, L. Crowhurst, A. Dolan, M. Lui, N. H. Hassan, J. P. Hallett, P. A. Hunt, H. Niedermeyer, J. M. Perez-Arlandis, M. Schrems, T. Welton and R. Wilding, *Phys. Chem. Chem. Phys.*, 2011, **13**, 16831–16840.
- 50 A. Pandey, R. Rai, M. Pala and S. Pandey, *Phys. Chem. Chem. Phys.*, 2014, **16**, 1559–1568.
- 51 Y.-D. Song, Q. T. Wang and L. Chen, *J. Phys. Org. Chem.*, 2023, **36**, e4474.
- 52 R. K. Venkatraman and A. J. Orr-Ewing, *Acc. Chem. Res.*, 2021, **54**, 4383–4394.
- 53 Q. Zhou, M. Zhou, Y. Wei, X. Zhou, S. Liu, S. Zhang and B. Zhang, *Phys. Chem. Chem. Phys.*, 2017, **19**, 1516–1525.
- 54 J. Mei, N. L. C. Leung, R. T. K. Kwok, J. W. Y. Lam and B. Z. Tang, *Chem. Rev.*, 2015, **115**, 11718–11940.
- 55 S. Suzuki, S. Sasaki, A. S. Sairi, R. Iwai, B. Z. Tang and G. Konishi, *Angew. Chem., Int. Ed.*, 2020, **59**, 9856–9867.
- 56 C. Gao, L. Fu, J. Wang, Y. Chu, L. Gao, H. Qiu and J. Chen, *Chem. Biomed. Imaging*, 2025, **3**, 837–848.
- 57 A. Banerjee, K. De and U. Bhattacharjee, *J. Phys. Chem. B*, 2024, **128**, 849–856.
- 58 C. R. Benson, L. Kacenauskaite, K. L. VanDenburgh, W. Zhao, B. Qiao, T. Sadhukhan, M. Pink, J. Chen, S. Borgi, C.-H. Chen, B. J. Davis, Y. C. Simon, K. Raghavachari, B. W. Laursen and A. H. Flood, *Chem*, 2020, **6**, 1978–1997.
- 59 X. Ma, R. Sun, J. Cheng, J. Liu, F. Gou, H. Xiang and X. Zhou, *J. Chem. Educ.*, 2016, **93**, 345–350.
- 60 Y. Huang, J. Xing, Q. Gong, L.-C. Chen, G. Liu, C. Yao, Z. Wang, H.-L. Zhang, Z. Chen and Q. Zhang, *Nat. Commun.*, 2019, **10**, 169.
- 61 J. T. Edward, *J. Chem. Educ.*, 1970, **47**, 261.
- 62 C. Y. Victor Gray, J. Mårtensson and K. Börjesson, *J. Am. Chem. Soc.*, 2019, **141**, 9578–9584.
- 63 A. A. Veldhorst and M. C. C. Ribeiro, *J. Chem. Phys.*, 2018, **148**, 193803.
- 64 Y. L. Wang, B. Li, S. Sarman, F. Mocci, Z.-Y. Lu, J. Yuan, A. Laaksonen and M. D. Fayer, *Chem. Rev.*, 2020, **120**, 5798–5877.
- 65 R. Clark, M. A. Nawawi, A. Dobre, D. Pugh, Q. Liu, A. P. Ivanov, A. J. P. White, J. B. Edel, M. K. Kuimova, A. J. S. McIntosh and T. Welton, *Chem. Sci.*, 2020, **11**, 6121–6133.



- 66 S. Chatterjee, S. H. Deshmukh and S. Bagchi, *J. Phys. Chem. B*, 2022, **126**, 8331–8337.
- 67 L. Naimovičius, M. Dapkevičius, E. Radiunas, M. Miroshnichenko, G. Kreiza, C. Alcaide, P. Baronas, Y. Sasaki, N. Yanai, N. Kimizuka, A. B. Pun, M. Solà, P. Bharmoria, K. Kazlauskas and K. Moth-Poulsen, *Chem. Sci.*, 2025, **16**, 20255–20264.
- 68 H. Kouno, Y. Sasaki, N. Yanai and N. Kimizuka, *Chem. – Eur. J.*, 2019, **25**, 6042.
- 69 P. Bharmoria, S. Hisamitsu, H. Nagatomi, T. Ogawa, M.-A. Morikawa, N. Yanai and N. Kimizuka, *J. Am. Chem. Soc.*, 2018, **34**, 10848–10855.
- 70 P. Bharmoria, S. Hisamitsu, Y. Sasaki, T. S. Kang, M.-A. Morikawa, B. Joarder, K. Moth-Poulsen, H. Bildirir, A. Mårtensson, N. Yanai and N. Kimizuka, *J. Mater. Chem. C*, 2021, **9**, 11655–11661.
- 71 F. J. Morgan and H. Dugan, *Appl. Opt.*, 1979, **18**, 4112–4115.
- 72 A. Muratsugu, J. Watanabe and S. Kinoshita, *J. Chem. Phys.*, 2014, **140**, 214508.
- 73 A. Raj, P. Verma, A. Beliaev, P. Myllyperkiö and T. Kumpulainen, *Chem. Sci.*, 2025, **16**, 13935–13943.
- 74 F. Serra and E. M. Terentjev, *Macromolecules*, 2008, **41**, 981–986.
- 75 M. W. Dale, D. J. Cheney, C. Vallotto and C. J. Wedge, *Phys. Chem. Chem. Phys.*, 2020, **22**, 28173–28182.
- 76 N. Gao, Y. Yang, Z. Wang, X. Guo, S. Jiang, J. Li, Y. Hu, Z. Liu and C. Xu, *Chem. Rev.*, 2024, **124**, 27–123.
- 77 L. V. T. D. de Alencar, S. B. Rodríguez-Reartes, F. W. Tavares and F. Llovel, *ACS Sustainable Chem. Eng.*, 2024, **12**, 7987–8000.
- 78 T. S. Kang, M.-A. Morikawa, M. Singh and N. Kimizuka, *J. Am. Chem. Soc.*, 2025, **147**, 8809–8819.
- 79 M. Mahato, Y. Murakami and S. K. Das, *Appl. Mater. Today*, 2023, **32**, 101808.
- 80 Y. Wang, *J. Phys. Chem. B*, 2009, **113**, 11058–11060.
- 81 J. Leier, N. C. Michenfelder and A.-N. Unterreiner, *Chem. Open*, 2021, **10**, 72–82.
- 82 K. P. Rola, A. Zajac, A. Szpecht, D. Kowal, J. Cybińska, M. Śmiślak and K. Komorowska, *Eur. Polym. J.*, 2021, **156**, 110615.
- 83 T. S. Groves and S. Perkin, *Faraday Discuss.*, 2024, **253**, 193–211.
- 84 I. Tanabe, Y. Kurawaki, Y. Morisawa and Y. Ozaki, *Phys. Chem. Chem. Phys.*, 2016, **18**, 22526–22530.
- 85 A. P. Demchenko, *Luminescence*, 2002, **17**, 19–42.
- 86 W. C. Galley and R. M. Purkey, *Proc. Natl. Acad. Sci. U. S. A.*, 1970, **67**, 1116–1121.
- 87 A. P. Demchenko, *Biophys. Chem.*, 1982, **15**, 101–109.
- 88 A. Paul, P. K. Mandal and A. Samanta, *J. Phys. Chem. B*, 2005, **109**, 9148–9153.
- 89 Z. Hu and C. J. Margulis, *Acc. Chem. Res.*, 2007, **40**, 1097–1105.
- 90 T. Singh and A. Kumar, *J. Phys. Chem. B*, 2008, **112**, 4079–4086.
- 91 *Red-Edge Excitation Spectroscopy of Proteins with the FS5 Spectrofluorometer*, Edinburgh Instruments Ltd., 2014. [https://www.edinst.com/wp-content/uploads/2018/06/Red-Edge-Excitation-Proteins\\_App16.pdf](https://www.edinst.com/wp-content/uploads/2018/06/Red-Edge-Excitation-Proteins_App16.pdf).
- 92 F. van Rantwijk and R. A. Sheldon, *Chem. Rev.*, 2007, **107**, 2757–2785.
- 93 I. Bandrés, M. Haro, B. Giner, H. Artigas and C. Lafuente, *Phys. Chem. Liq.*, 2011, **49**, 192–205.
- 94 H. Guo, Q. Yu, Y. Xiong and F. Yang, *J. Mol. Liq.*, 2021, **335**, 116179.
- 95 C. Feng, K. Zhang, B. Zhang, L. Feng, L. He, C.-F. Chen and M. Li, *Angew. Chem., Int. Ed.*, 2025, **64**, e202425094.
- 96 G. Longhi, E. Castiglioni, J. Koshoubu and G. S. Abbate, *Chirality*, 2016, **28**, 696–707.
- 97 B. Zercher and T. A. Hopkins, *Inorg. Chem.*, 2016, **55**, 10899–10906.
- 98 Z. Huang, M. Yi, Y. Xu, P. Qi, Y. Liu, A. Song and J. Hao, *J. Mater. Chem. C*, 2021, **9**, 13276.
- 99 V. Morad, K. M. McCall, K. Sakhatskyi, E. Lehmann, B. Walfort, A. S. Losko, P. Trtik, M. Strobl, S. Yakunin and M. V. Kovalenko, *ACS Photonics*, 2021, **8**, 3357–3364.
- 100 T. Mizuta, K. Sueyoshi, T. Endo and H. Hisamoto, *Anal. Chem.*, 2021, **93**, 4143–4148.
- 101 S. Hisamitsu, N. Yanai and N. Kimizuka, *Angew. Chem., Int. Ed.*, 2015, **54**, 11550–11554.
- 102 S. Hisamitsu, N. Yanai, H. Kouno, E. Magome, M. Matsuki, T. Yamada, A. Monguzzi and N. Kimizuka, *Phys. Chem. Chem. Phys.*, 2018, **20**, 3233–3240.
- 103 S. Hisamitsu, J. Miyano, K. Okumura, J. K.-H. Hui, N. Yanai and N. Kimizuka, *Chem. Open*, 2020, **9**, 14–17.
- 104 K. Shimizu, S. Hisamitsu, N. Yanai, N. Kimizuka and J. N. C. Lopes, *J. Phys. Chem. B*, 2020, **124**, 3137–3144.
- 105 R. Kupfer, F. Wang, J. F. Wishart, M. Babzien, M. N. Polyanskiy, I. V. Pogorelsky, T. Rao, L. Cultrera, N. Vafaei-Najafabadi and M. A. Palmer, *Phys. Rev. Appl.*, 2023, **19**, 014052.
- 106 H. Zhang, C. Zhang, S. Vaziri, F. Kenarangi and Y. Sun, *IEEE Photonics J.*, 2021, **13**, 1500308.
- 107 A. N. Oraevsky, *Quantum Electron.*, 2002, **32**, 377.
- 108 T. Reynolds, N. Riesen, A. Meldrum, X. Fan, J. M. M. Hall, T. M. Monro and A. François, *Laser Photonics Rev.*, 2017, **11**, 1600265.
- 109 X. He, Q. Shao, P. Cao, W. Kong, J. Sun, X. Zhang and Y. Deng, *Lab Chip*, 2015, **15**, 1311–1319.
- 110 E. F. Borra, O. Seddiki, R. Angel, D. Eisenstein, P. Hickson, K. R. Seddon and S. P. Worden, *Nature*, 2007, **447**, 979–981.
- 111 E. Hecht, *Optics*, Pearson Education, 4th edn, 2001.
- 112 M. Tariq, M. G. Freire, B. Saramago, J. A. P. Coutinho, J. N. C. Lopes and L. P. N. Rebelo, *Chem. Soc. Rev.*, 2012, **41**, 829–868.
- 113 T. Szobody, *Reflecting the future: Revolutionizing space exploration with liquid mirrors*, NC Space Grant News, 2024.
- 114 N. Rowlands, Á. Romero-Calvo, D. Strafford, R. Kamire, A. Childers, S. F. Yates, E. Rahislic, J. Smoke, S.-H. Zheng, P. Cameron, G. Cano-Gómez, H. Chen, T. Hu, E. Comstock and M. Herrada, *Proc. SPIE*, 2024, 13100, Advances in Optical and Mechanical Technologies for Telescopes and Instrumentation VI, 131007H.



- 115 X. Hou, Z. Wang, Z. Zheng, J. Guo, Z. Sun and F. Yan, *ACS Appl. Mater. Interfaces*, 2019, **11**, 20417–20424.
- 116 I. Bandrés, M. Haro, B. Giner, H. Artigas and C. Lafuente, *Phys. Chem. Liq.*, 2011, **49**, 192–205.
- 117 H. Lin, P. W. Oliveira and M. Veith, *Appl. Phys. Lett.*, 2008, **93**, 141101.
- 118 H. Lin, P. W. de Oliveira and M. Veith, *Opt. Mater.*, 2011, **33**, 759–762.
- 119 Y. Chen, D. Zhao, Y. Bai, Y. Duan, C. Liu, J. Gu, X. Wang, X. Sun, Y. Li and L. Zhang, *J. Mol. Liq.*, 2022, **348**, 118031.
- 120 J. Luan, Y. Cheng, F. Xue, L. Cui and D. Wang, *ACS Omega*, 2023, **8**, 25582–25591.
- 121 E. Ferreira, G. Ramos-Ortiz, A. Vazquez and M. Trejo-Durán, *J. Mol. Liq.*, 2023, **384**, 122253.
- 122 I. Betka, *Nonlinear optical refractive index measurements of pure water via Z-scan technique at 800 nm*, *arXiv*, 2025, preprint, arXiv:2502.02944, DOI: [10.48550/arXiv.2502.02944](https://doi.org/10.48550/arXiv.2502.02944).
- 123 P. L. Rall, D. Förster, T. Graf and C. Pflaum, *Opt. Express*, 2022, **30**, 38643–38662.
- 124 S. M. Patil, S. K. Gupta, D. Goswami and R. Gupta, *ACS Omega*, 2023, **8**, 32444–32449.
- 125 L. V. Elzen and T. A. Hopkins, *ACS Sustainable Chem. Eng.*, 2019, **7**, 16690–16697.
- 126 B. Nelson, L. V. Elzen, G. Whitacre and T. A. Hopkins, *ChemPhotoChem*, 2021, **5**, 1071–1078.
- 127 C. R. Wright, L. V. Elzen and T. A. Hopkins, *J. Phys. Chem. B*, 2018, **122**, 8730–8737.
- 128 Y. Murakami, S. K. Das, Y. Himuro and S. Maeda, *Phys. Chem. Chem. Phys.*, 2017, **19**, 30603–30615.
- 129 V. Khokhar, Deepika and S. Pandey, *J. Photochem. Photobiol., A*, 2022, **427**, 113798.
- 130 Sangeeta, A. Sil, V. Singh, R. Bhati and B. Guchhait, *J. Phys. Chem. B*, 2024, **128**, 9805–9814.
- 131 P. Zhou and K. Han, *Acc. Chem. Res.*, 2018, **51**(7), 1681–1690.
- 132 Z. Usmani, M. Sharma, M. Tripathi, T. Lukk, Y. Karpichev, N. Gathergood, B. N. Singh, V. K. Thakur, M. Tabatabaei and V. K. Gupta, *Sci. Total Environ.*, 2023, **88**, 163002.
- 133 K. L. Kelly, E. Coronado, L. L. Zhao and G. C. Schatz, *J. Phys. Chem. B*, 2003, **107**, 668–677.
- 134 U. Banin, Y. Ben-Shahar and K. Vinokurov, *Chem. Mater.*, 2014, **26**, 97–110.
- 135 M. Bhar, N. Bhunia, G. H. Debnath, D. H. Waldeck and P. Mukherjee, *Chem. Phys. Rev.*, 2024, **5**, 011306.
- 136 J. Chang, H. Chen, G. Wang, B. Wang, X. Chena and H. Yuan, *RSC Adv.*, 2019, **9**, 7015–7024.
- 137 T. Antrack, M. Kroll, M. Sudzius, C. Cho, P. Imbrasas, M. Albaladejo-Siguan, J. Benduhn, L. Merten, A. Hinderhofer, F. Schreiber, S. Reineke, Y. Vaynzof and K. Leo, *Adv. Sci.*, 2022, **9**, 2200379.
- 138 F. Migliorini, S. Belmuso, R. Dondè, S. D. Iuliis and I. Altman, *Carbon Trend.*, 2022, **8**, 100184.
- 139 N. Tarasenko, A. Stupak, N. Tarasenko, S. Chakrabarti and D. Mariotti, *ChemPhysChem*, 2017, **18**, 1074–1083.
- 140 R. Jiang, Y. Guo and X. Guo, *Sol. Energy Mater. Sol. Cells*, 2026, **294**, 113934.
- 141 Y. U. Paulechka, A. G. Kabo, A. V. Blokhin, G. J. Kabo and M. P. Shevelyova, *J. Chem. Eng. Data*, 2010, **55**, 2719–2724.
- 142 B. D. Rabideau, K. N. West and J. H. Davis, Jr., *Chem. Commun.*, 2018, **54**, 5019–5031.
- 143 P. Dehury, J. Singh and T. Banerjee, *ACS Omega*, 2018, **3**, 18016–18027.
- 144 E. Sperling, Mapping the Impact of heat on photonics, Semiconductor Engineering 2019, <https://semiengineer.com/mapping-the-impact-of-heat-on-light/>.
- 145 Q. Jin, K. Williams, E. Yiwen, J. Dai and X. Zhang, Observation of broadband terahertz wave generation from liquid water, in Nonlinear Optics, OSA Technical Digest (online) (Optica Publishing Group, 2017), paper NW3A.1.
- 146 Q. Jin, Y. W. E, J. M. Dai, L. L. Zhang, C. L. Zhang, A. Tcypkin, S. Kozlov and X. Zhang, Terahertz photonics in liquids, in Nonlinear Optics (NLO), OSA Technical Digest (Optica Publishing Group, 2019), paper NTu2B.3.
- 147 P. Q. Liu, X. Miao and S. Datta, *Opt. Mater. Express*, 2023, **13**, 699–727.
- 148 P. C. Wu, T.-H. Kim, A. S. Brown, M. Losurdo, G. Bruno and H. O. Everitt, *Appl. Phys. Lett.*, 2007, **90**, 103119.
- 149 C. Kunkel, J. T. Margraf, K. Chen, H. Oberhofer and K. Reuter, *Nat. Commun.*, 2021, **12**, 2422.
- 150 C. Wang, H. Dong, L. Jiang and W. Hu, *Chem. Soc. Rev.*, 2018, **47**, 422–500.
- 151 A. Chelsea, Are Liquid Solar Panels the Next Big Thing in Solar Power? Green Lancer, 2024, <https://www.greenlancer.com/post/liquid-solar>.
- 152 P. V. Kamat, K. Tvrđy, D. R. Baker and E. J. Radich, *Chem. Rev.*, 2010, **110**, 6664–6688.
- 153 T. Ullrich, D. Munz and D. M. Guldi, *Chem. Soc. Rev.*, 2021, **50**, 3485–3518.
- 154 P. Bharmoria, H. Bildirir and K. Moth-Poulsen, *Chem. Soc. Rev.*, 2020, **49**, 6529–6554.
- 155 V. Sharma, R. Suthar, S. Karak and A. Sinha, *ACS Appl. Opt. Mater.*, 2025, **3**, 259–271.
- 156 W. G. J. H. M. van Sark, K. W. J. Barnham, L. H. Slooff, A. J. Chatten, A. Büchtemann, A. Meyer, S. J. McCormack, R. Koole, D. J. Farrell, R. Bose, E. E. Bende, A. R. Burgers, T. Budel, J. Quilitz, M. Kennedy, T. Meyer, C. D. M. Donegá, A. Meijerink and D. Vanmaekelbergh, *Opt. Express*, 2008, **16**, 21773–21792.
- 157 L. Naimovičius, P. Bharmoria and K. Moth-Poulsen, *Mater. Chem. Front.*, 2023, **7**, 2297–2315.
- 158 B. Daiber, K. van den Hoven, M. H. Futscher and B. Ehrler, *ACS Energy Lett.*, 2021, **6**, 2800–2808.
- 159 D. Nguyen, T. Van Huynh, V. S. Nguyen, P.-L. D. Cao, H. T. Nguyen, T.-C. Wei, P. H. Tran and P. T. Nguyen, *RSC Adv.*, 2021, **11**, 21560–21566.
- 160 D. Nguyen, M. T. Nguyen, T. T. D. Nguyen, V. T. Huynh, B. P. N. Nguyen and P. T. Nguyen, *Aust. Ceram. Soc.*, 2022, **58**, 913–921.
- 161 M. Gorlova and L. Kloo, *Dalton Trans.*, 2008, 2655–2666.
- 162 M. Hassan, T. A. Shifa, A. Vomiero, E. Moretti and K. B. Ibrahim, *Small*, 2025, **21**, e09030.



- 163 S. Fernandes, J. C. G. E. da Silva and L. P. da Silva, *Materials*, 2022, **15**, 3446.
- 164 C. Yang, H. A. Atwater, M. A. Baldo, D. Baran, C. J. Barile, M. C. Barr, M. Bates, M. G. Bawendi, M. R. Bergren, B. Borhan, C. J. Brabec, S. Brovelli, V. Bulovic, P. Ceroni, M. G. Debije, J.-M. Delgado-Sanchez, W.-J. Dong, P. M. Duxbury, R. C. Evans, S. R. Forrest, D. R. Gamelin, N. C. Giebink, X. Gong, G. Griffini, F. Guo, C. K. Herrera, A. W. Y. Ho-Baillie, R. J. Holmes, S.-K. Hong and T. Kirchartz, *et al.*, *Joule*, 2022, **6**, 8.
- 165 M. Mokhtarpour, A. Rostami, H. Shekaari, A. Zarghami and S. Faraji, *Sci. Rep.*, 2023, **13**, 18936.
- 166 S. L. Piper, M. Kar, D. R. MacFarlane, K. Matuszek and J. M. Pringle, *Green Chem.*, 2022, **24**, 102–117.
- 167 M. Królikowski, M. Więckowski, K. Żółtańska and M. Królikowska, *J. Chem. Eng. Data*, 2024, **69**, 958–972.
- 168 Z. Wang, A. Roffey, R. Losantos, A. Lennartson, M. Jevric, A. U. Petersen, M. Quant, A. Dreos, X. Wen, D. Sampedro, K. Börjesson and K. Moth-Poulsen, *Energy Environ. Sci.*, 2019, **12**, 187–193.
- 169 Z. Wang, H. Hölzel and K. Moth-Poulsen, *Chem. Soc. Rev.*, 2022, **51**, 7313–7326.
- 170 X. Xu and G. Wang, *Small*, 2022, **18**, e2107473.
- 171 X. Xu, C. Li, W. Li, J. Feng and W.-Y. Li, *Energy Environ. Sci.*, 2025, **18**, 8990–9017.
- 172 N. Baggi, H. Hölzel, H. Schomaker, K. Moreno and K. Moth-Poulsen, *ChemSusChem*, 2023, **17**, ge202301184.
- 173 N. Baggi, L. M. Muhammad, Z. Liasi, J. L. Elholm, P. Baronas, E. Molins, K. V. Mikkelsen and K. Moth-Poulsen, *J. Mater. Chem. A*, 2024, **12**, 26457–26464.
- 174 L. Fernandez, H. Hölzel, P. Ferreira, N. Baggi, K. Moreno, Z. Wang and K. Moth-Poulsen, Surfactant-enabled strategy for molecular solar thermal energy storage systems in water, *Green Chem.*, 2025, **27**, 14119–14130.

